

Article

The Effects of River Torrents and Debris on Historic Masonry Vaulted Arch Bridges

Philippe Van Bogaert * and Hans De Backer 

Civil Engineering Department, Ghent University, 9052 Ghent, Belgium; hans.debacker@ugent.be

* Correspondence: philippe.vanbogaert@ugent.be

Abstract: The carrying capacity for vertical loads of well-maintained masonry arch bridges is reasonably high. This might not be the case for horizontal loads, the effects of which have not been the subject of extensive research aside from seismic occurrences. Arch bridges crossing rivers are subjected to sudden horizontal loads, due to river torrents, carrying debris from higher grounds. The magnitude of these horizontal loads is similar to those of coastal waves and debris; however, their effect on these structures has yet to be explored in detail. The narrow and high Devil's Bridge across the Arda River (BG) and the wide, low Candia Viaduct across the Sesia River (I) were chosen as examples. Both are strongly exposed to fast-washing flow in the river during spring. FE simulations show that the impact of the rapidly rising river water influences the general stability, while the effect of debris mainly causes local damage. The results exhibit that tall, slender masonry arch structures fail due to the brittle fracture of the material, followed by the shear failure of a pier body. In contrast, lower and wider viaducts fail due to exaggerated tensile cracking in the upstream parts of a pier and the associated increasing pressure at its downstream parts.

Keywords: masonry arch bridge; torrent river wave; debris; pier slenderness; masonry shear; FE simulation of failure



Citation: Van Bogaert, P.; De Backer, H. The Effects of River Torrents and Debris on Historic Masonry Vaulted Arch Bridges. *Buildings* **2024**, *14*, 54. <https://doi.org/10.3390/buildings14010054>

Academic Editor: Panagiotis Stylianidis

Received: 8 November 2023

Revised: 20 December 2023

Accepted: 21 December 2023

Published: 24 December 2023



Copyright: © 2023 by the authors. Licensee MDPI, Basel, Switzerland. This article is an open access article distributed under the terms and conditions of the Creative Commons Attribution (CC BY) license (<https://creativecommons.org/licenses/by/4.0/>).

1. Introduction

Since Roman times, and up to the past century, stone or brickwork vaulted arch bridges have been built and proved to be a reliable type of construction. In many European countries, they can still be found and serve as crossings of rivers, roads, and railways. If well maintained, the load-carrying capacity of these structures can be high, and failure mainly occurs suddenly, due to the abrupt detachment of the inner roll layer of the vault.

The remaining strength and stability of these types of bridges is a permanent concern, on the one hand, because many of them belong to the historic heritage and must therefore be preserved. On the other hand, because their condition degrades over time, restoration becomes necessary. Hence, effective methods are needed to regularly assess their load-carrying capacity. It is done frequently with regard to the vertical traffic load. For example, the load-bearing capacity of railway bridges was investigated with software SCIA (version 22) and MATLAB (version R2023b) [1]. The load-bearing capacity was assessed by carrying out measurements of the intrados in [2]. Limit analysis or a model with nondeformable blocks was implemented in [3], using the principle developed in [4]. Reliability-based structural assessment in the case of the Cernadela Bridge is exhibited in [5]. An extensive number of references for the methods and applications for vertical loads exist.

Significantly less research has been conducted with regard to horizontal loads. The main focus is on horizontal actions due to seismic phenomena. The dynamic response of the Ponte delle Torri Viaduct and the damage caused by the recent earthquake were investigated in [6]. Cyclic push-over analysis with the effect of natural seismic spectra was carried out in [7]. Seismic effects in the longitudinal direction of the bridge were examined

in [8], with masonry considered a perfectly plastic material. The inertia of the filling on the top of the vault was found to significantly contribute to the seismic effect.

In [9], static and dynamic tests were performed to determine the strength of masonry arches against horizontal loads. Taking the actual geometry as a starting point, the horizontal capacity of single-span masonry bridges with intrados strengthened with FRCM was studied in [10]. The Coulomb friction was also taken into account, which appeared to have an important influence. The lateral loading on masonry arch bridges was studied in [11]. In particular, the authors investigated the effect of ground pressure and ground cover at the top of the arch, as well as arches with a small rise-to-span ratio.

In an important contribution [12], the structural response of a typical masonry arch bridge to flood flow and debris was researched. Simulations were performed of the water pressure imposed on piers and abutments using the smoothed particle hydrodynamics method and the so-called macro-model to simulate masonry. The conclusion is mainly that spandrel walls and retaining walls on top of the arch are the most critical areas.

The aim of this research is to determine the strength of masonry vaulted arch bridges with regard to river floods and debris. In addition, the effects of the flood wave and the debris are considered separately, because the first is a distributed load, and the second is a local load. Finally, the aim is to determine the fracture mechanism through which such a bridge can fail. Although two different bridges are considered as the subject of the research, a parametric study is performed, thus allowing us to present the results in a more general context.

2. Materials and Methods

Obviously, masonry or brickwork is an inhomogeneous material. Merely to give an idea of this, the gneiss stones from Devil's Bridge (Bulgaria), discussed in Section 4, are reputed to have a compression strength of 37.84 MPa, whereas lime mortar has an average limit strength of 1.12 MPa. In general, bricks and stone are the resisting parts of masonry, whereas mortar is the softer substance. The thickness of the joints is an important factor. The joints spread the local contact between stones, thus obtaining a more equal load transfer. Yet, they constitute the weakest element of masonry. According to EN 1996-1-1 [13], Section 3.6.1.2, the compression strength of masonry is determined using Equation (1).

$$f_k = K f_b^\alpha f_m^\beta \quad (1)$$

In Equation (1), f_k is the characteristic value of the compression strength of the masonry, f_b is the normalized mean value of the compression strength of the bricks or stones, and f_m is the compression strength of the mortar. The values of the parameters of Equation (1) can be found in the aforementioned code. The equation reduces to a simpler form if the joint width deviates from standard practice. Moreover, the contact between mortar and stone exhibits poor shear resistance. This is generally expressed by using a reduced spring constant as in Equation (2), with u considered the displacement.

$$\sigma = k^n u \quad (2)$$

A similar relation applies to the shear stress, as exhibited in Equation (3).

$$\tau = k^{ms} \delta \quad (3)$$

In Equation (3), δ is the tangent slip of the contact surface. The shear strength of the contact surface depends linearly on the contact normal stress as in Equation (4). This equation is exactly as that used in the Mohr–Coulomb method.

$$f_s = \sigma \tan \varphi + c \quad (4)$$

The Mohr–Coulomb stress–strain relation is used widely in most software programs as a constitutive relation for masonry. In fact, it is a linear envelope from the plot that exhibits

the relation between shear and normal stress, as shown in Figure 1. As an alternative, the Drucker–Prager failure criterion may be considered. This also applies well to brittle material and is a smoother version of the Mohr–Coulomb law. In fact, it shows some resemblance to the von Mises criterion.

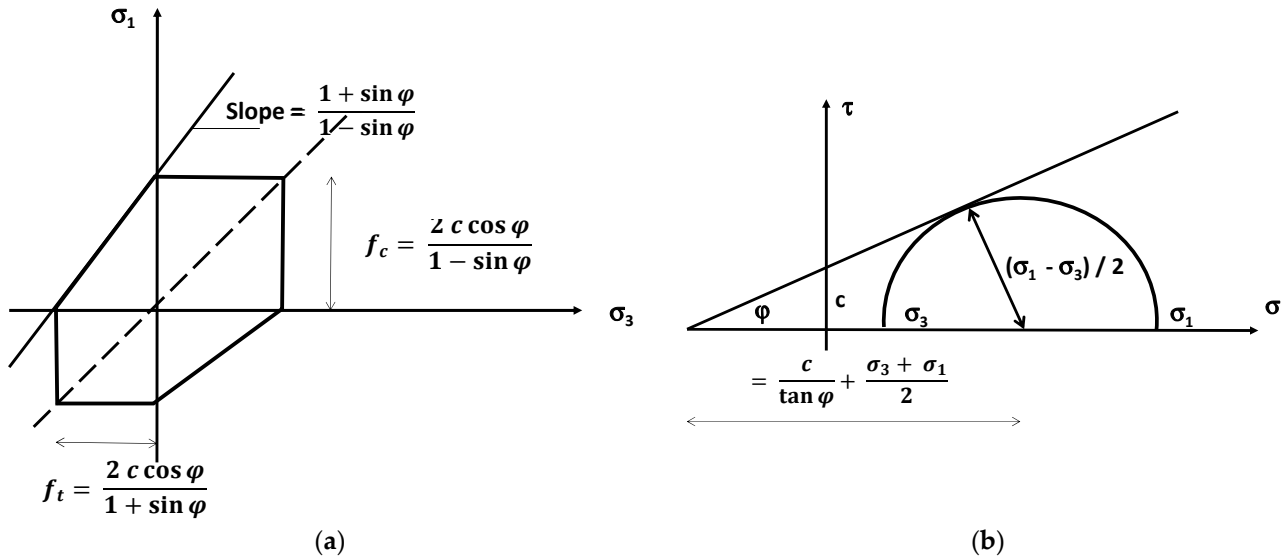


Figure 1. Mohr–Coulomb criteria: (a) normal stresses; (b) normal and shear stress.

However, the problem of applying the Mohr–Coulomb model to masonry becomes obvious. A typical situation would be that $f_c = 10 f_t$ and that $\tau = 0.3 f_c$. The first condition can be easily satisfied by having a steep slope of the indicated type. This is, however, not compatible with the second condition, since tension stress causes the value of c to be immensely high, and the shear resistance is increasing beyond reality. This proves that the Mohr–Coulomb criterion certainly is not perfect or even not adapted to masonry. A well-adapted scheme would have less interaction between normal stress in various directions, or even make them independent. In fact, the stress–strain relation should be similar to the one in Figure 2, which includes a sudden drop in resistance, once the maximum compression strength f_{cu} or minimum tension strength f_{ct} is reached.

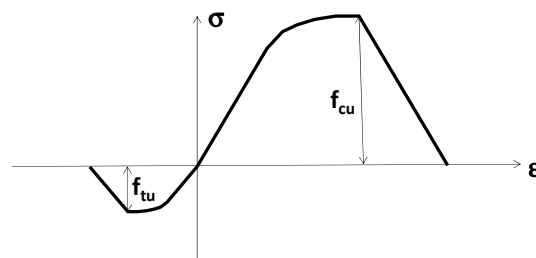


Figure 2. Stress–strain curve with strain softening.

Unfortunately, this type of stress–strain curve requires large computing effort, mostly beyond a reasonable limit. In addition, the graph does not include the characteristics of the contact layer between stones and mortar. Because of this, simplified models are often used [14]. The full micro-model, including nonlinear characteristics of stones, mortar, and the interface shown in Figure 3a, may be replaced by suppressing the interface conditions, thus creating a continuous micro-model, which is already less demanding, as exhibited in Figure 3b. A further step is to consider a discrete macro-model of several stones and mortar joints as a nonlinear solid, as shown in Figure 3c. According to the literature, the latter model is rather efficient, provided the out-of-plane effects are limited.

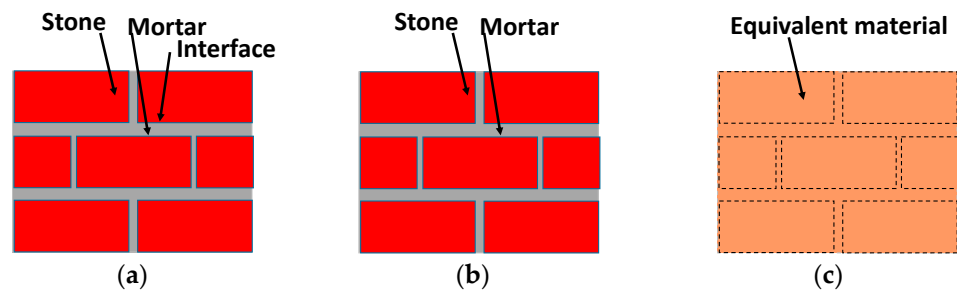


Figure 3. Types of FE modeling of masonry: (a) micro-model; (b) meso-model; (c) macro-model.

Building FE models of a solid structure raises the choice of the element type. As was previously implied, the general opinion is that volume elements best simulate solid structures. However, the question that arises is whether their use is indispensable. If chosen well, a model of a bridge pier, based on intersecting Mindlin plate elements, might perfectly be capable of simulating the behavior of this structure. This is the first option considered in the examples presented in subsequent sections. In addition, any real material characteristic is not considered since the values are varied to allow the assessment of their influence.

3. Lateral Load Due to River Torrents and Debris

The impact of sea waves on structures along seashores has been discussed extensively, both experimentally and theoretically. Many laboratories have contributed to finding appropriate equations and values for wave impact on vertical smooth structures. An important parameter is the return period of the storm that causes the wave. Most researchers promote the use of a 1000-year storm, which means a prediction is made to find four storms with the highest impact during that period. All kinds of probability distributions are assumed, varying from lognormal to Rayleigh, Weibull, Pareto, exponential, and normal distributions. Finally, the average of the four predicted values is taken.

These results are not directly applicable to the case of river torrents. For waves in coastal areas, a distribution of the pressure is found that closely resembles a hydrostatic, i.e., triangular distribution, which was found in a previous experimental study by measuring at eight points along a vertical line indicating the storm barrier [15]. This is indicated in Figure 4a, which shows that the distribution is almost triangular. For the case of water-retaining walls along the Scheldt River in Antwerp, recommendations from German standards were considered [16].

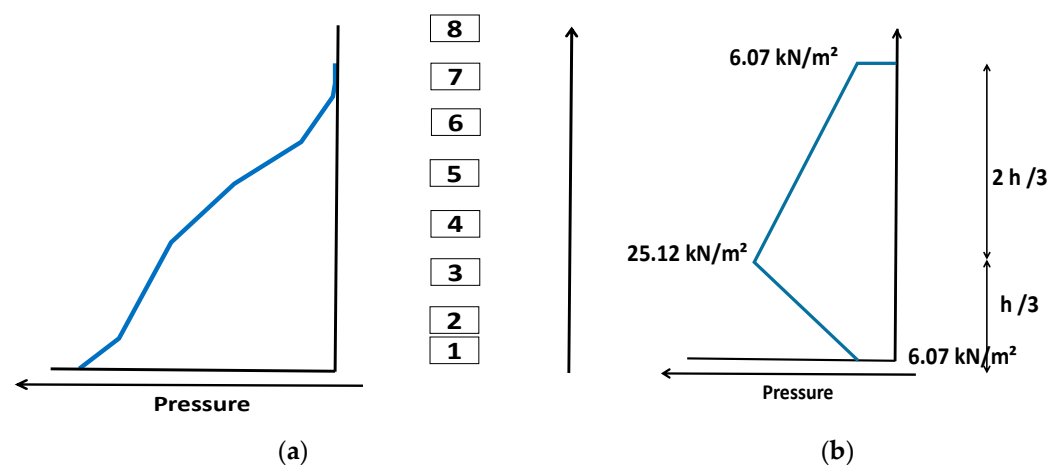


Figure 4. Pressure distribution due to torrent waves: (a) experimental curve; (b) adopted curve.

In contrast to the previous study, a distribution with the height of the pressure due to river torrents is given, which rather resembles a pentagon, as shown in Figure 4b. As far as the lower part is concerned, there is a decrease in pressure toward the bottom, because a

hydrostatic back pressure is induced on the downstream side of the obstacle in the river. The top part of the pentagon exhibits no pressure, equal to zero at the top. This is completely normal if an overtopping is possible, with splashing water. This does not necessarily seem to be the case for a bridge pier. However, there may be a higher pressure on both sides of the pier, and there may still be splashes of water. For this reason, the scheme of the pentagon was used here, as indicated in Figure 4b. The magnitude of the pressure changes with the height of the torrent wave. The recommendations in [16] rely on the fact the vertical walls or piers are located in a river bed, but this bed has a really small slope. As a consequence, the waves are fully or partially reflected. This phenomenon was researched in [17]. The method relies on the second-order wave theory. The load distribution is based on the full reflection of the waves and nonbraking waves and corresponds to Figure 4b.

The calculation of the load due to debris is easier. A horizontal line load is considered, conventionally fixed at 1 m width. The intensity seems to be independent of the water level and amounts to 30 kN/m. Obviously, this load can act anywhere, and at several points, it must be assumed to be positive. A partial safety factor was not applied to any of these loads, because a failure condition was investigated here. The torrent wave has a global character, while the effect of debris is rather local. If a γ -factor is used, the reliability value varies from $\beta = 3.3$ to 4.3 depending on whether RC1 to RC3 is considered. The associated γ values then range from 1.31 to 1.44. In general, the value of 1.3 would already be very high for such an exceptional phenomenon.

4. Results of Case 1: Devil's Bridge (Bulgaria)

The Devil's Bridge crosses the Arda River near the town of Dyadovtshi; it was built from 1515 to 1518, replacing a Roman bridge. According to [18], this bridge has remarkable architecture from the Ottoman period. A particular characteristic is the small width of 3.4 m for a 65.7 m long and height of 12.2 m above the water level. The bridge is exhibited in Figure 5a in normal conditions.

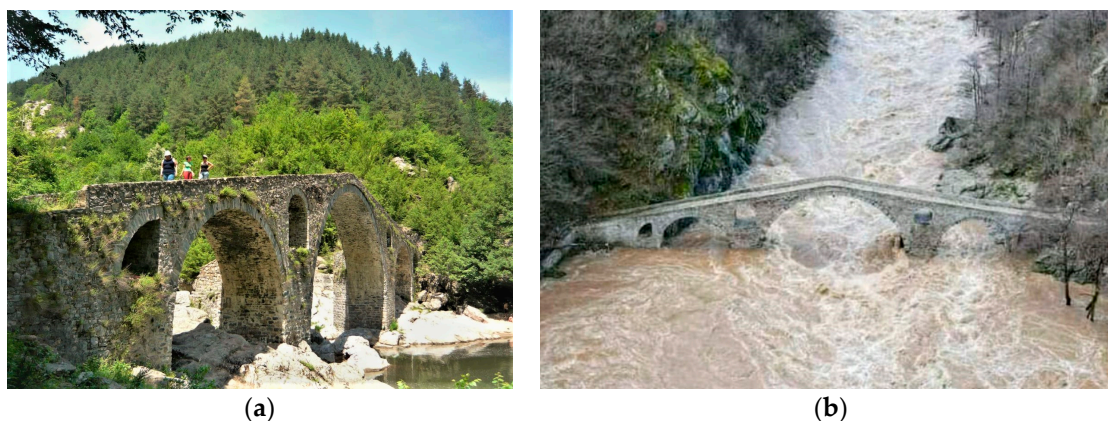


Figure 5. Devil's Bridge at different seasons: (a) bridge during summer time; (b) bridge under heavy river torrent.

Without a doubt, the load-carrying capacity related to traffic on this bridge is not the main concern. There can only be one lane on the bridge. Figure 5b illustrates how quickly rising river floods and, most likely, the debris carried by these torrents cause the main load effect. The piers of this bridge are therefore its weakest point. The two piers are marginally different in size. As such, attention was given to the largest pier. With respect to the debris load and torrent wave, statistical data [19] indicate that there are one to three annual torrents and that the largest recorded water level is 5.64 m.

Numerical simulations of masonry require considerable computer effort, especially when solid elements are used. Therefore, in a first approximation, plate elements were used, with the same resistance moment as the piers. Plate elements were also used for the vaults in this model. The constitutive relationship of Mohr–Coulomb was assumed for the

material. Figure 6a exhibits the model with plate elements, and Figure 6b shows a detail of the largest pier.

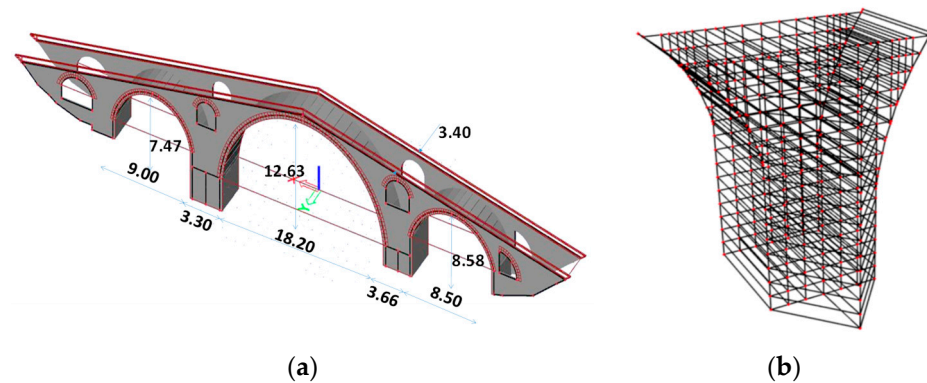


Figure 6. Model of Devil's Bridge with plate elements: (a) model using plate elements (skew view); (b) pier composed of plate elements.

Some results of this approach are unexpected. The horizontal displacements of the vault increase significantly due to torrent waves from maximum water height, as can be seen in Figure 7. The most obvious failure mechanism, which was also expected here, consists of tensile stresses occurring on the upstream side of the piers, causing them to crack and increasing the pressure on the downstream side. This process continues, until either the pressure becomes too great, or there is a loss of global equilibrium. The result of such progressive degradation is shown in Figure 8a for the load induced by river torrent and in Figure 8b for the effect of debris. The value of y is the depth of the pier base, counted from downstream to upstream.

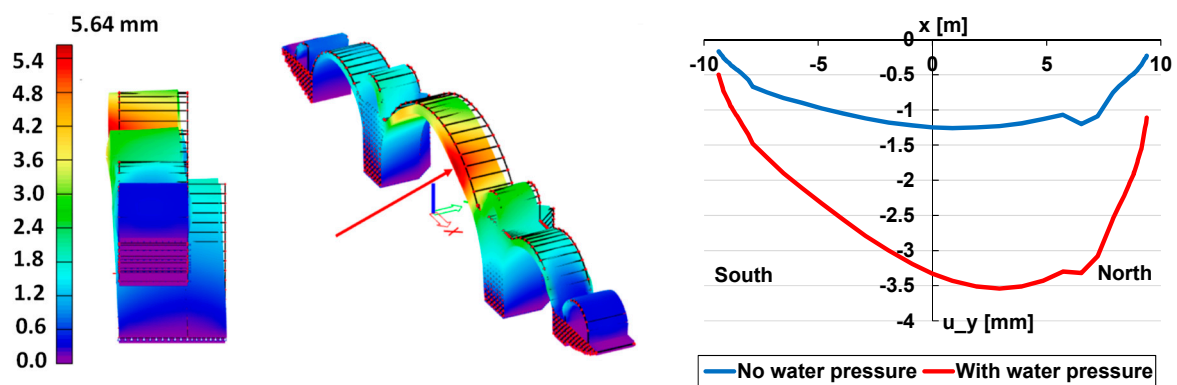


Figure 7. Vault displacements due to river torrent.

The blue lines always show the effect of all other loads, such as dead load and an eccentrically arranged traffic load, so that the greatest pressure is generated on the downstream side. It can be seen that the latter does not give rise to cracks at the base of the piers. This is also the case with the debris load. The horizontal loading caused by wave torrents does indicate cracks and increased pressure on the downstream side.

Unexpectedly, the amount of the failure load is independent of the brickwork's compressive strength. Because of this, the previously mentioned mechanism is unable to function. The failure moment of the pier is shown in Figure 9a as a function of f_c , the masonry's strength, for various values of the water height. Because the lever arm varies with each water height, the value of the bending moment may be more significant than the failure load. It can be seen from the graph that, at a small water height, the failure value still increases with f_c , but once a moderate height is considered, there is only a small increase. In that context, the graph of Figure 9b, which gives the horizontal displacements of the pier

top for $H = 5.67$ m as a function of f_c , is clearer. It becomes apparent that the displacements no longer increase appreciably as soon as $f_c = 4$ MPa. Displacements do not indicate a clear failure state but are useful for creating a Southwell plot [20]. As is known, the slope of the line of such a graph is inversely proportional to the failure load. For the different values of f_c , one finds almost perfect linear relationships with covariances ranging from 0.9964 to 0.9999. This method is therefore suitable for determining reliable values of the failure load.

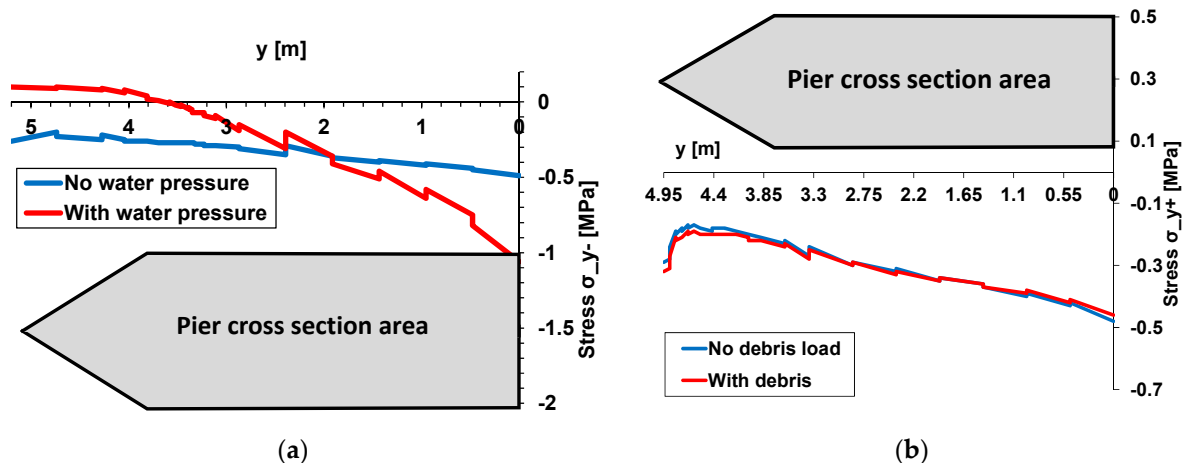


Figure 8. (a) Vertical stress at the pier base due to water pressure; (b) vertical stress at the pier base due to debris.

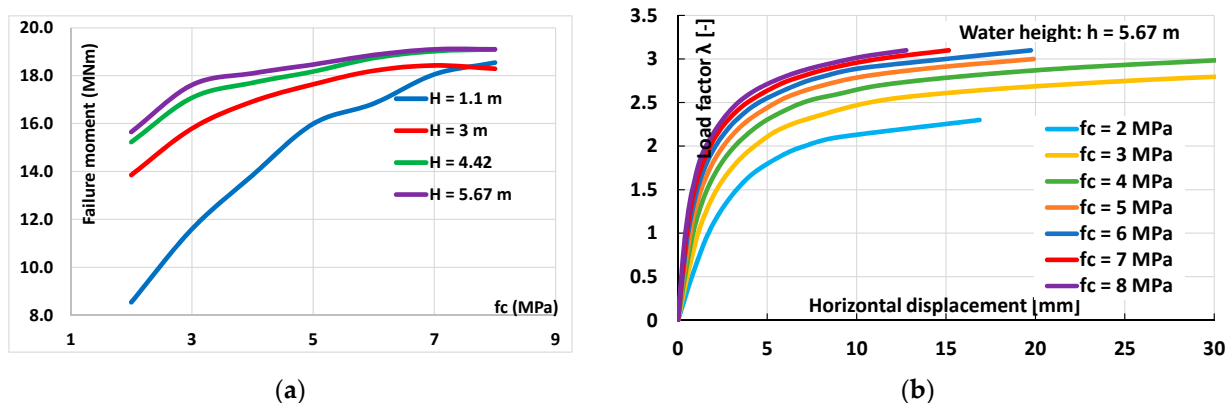


Figure 9. Failure load due to wave torrent: (a) failure load versus masonry strength; (b) failure load versus displacements.

The effect of debris is very different from that of the torrent wave. Debris is a local load, and the simulation clearly shows this as a result. For example, in Figure 10, the strains in the material are shown on the left, and on the right, the deformation due to an impact of debris of 900 kN is illustrated. This last value corresponds to the water height of 5.67 m. The fact that the impact of debris mainly exerts a local effect should not be interpreted as meaning that this is a negligible load, quite the contrary. The local destruction of masonry favors the general collapse mechanism, as is the case for the wave torrent, and accelerates the loss of equilibrium, especially in the section of the pier where the destruction is caused.

The conclusions of the results with this modeling therefore imply that failure occurs due to the lateral torrent wave load with the maximum water height and 2.3 times the amplitude of the wave. Excessive overturning causes cracking in the upstream part of the pier and a reduction in compressed area. If the compression strength exceeds 4 MPa, it has no further influence on the failure load.

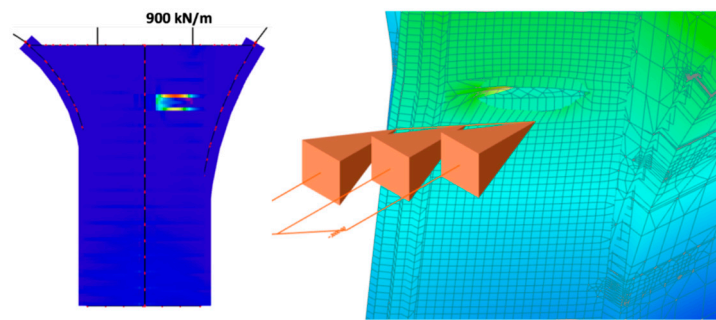


Figure 10. Effect of debris: (Left) local strains; (Right) deformation.

The fact that the failure load does not increase further for larger values of the masonry compressive strength raises some doubts about the completeness of the results and the mechanism of failure. Therefore, a more elaborate model was generated using solid elements, exhibited in Figure 11, and considering multiple constitutive relationships. These include the previously used Mohr–Coulomb equation with solid elements, the same elements with crack and plasticity or strain softening, and finally, a meso-model with brittle behavior. The graph in Figure 12 exhibits the displacements of the top of the pier as a function of a multiplier of the largest torrent wave load, corresponding to a water height of 5.67 m. Horizontal displacements are not relevant in themselves, but they do allow Southwell plots to be drawn, and thus a clear value of the failure load or a multiplication factor for the assumed load can be determined.

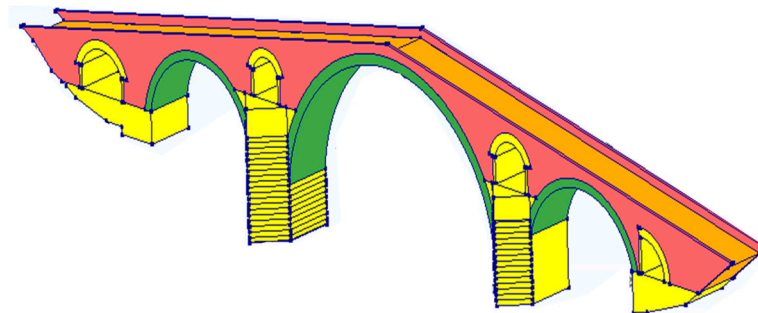


Figure 11. The 3D solid element model with mesh size 0.30 m for piers.

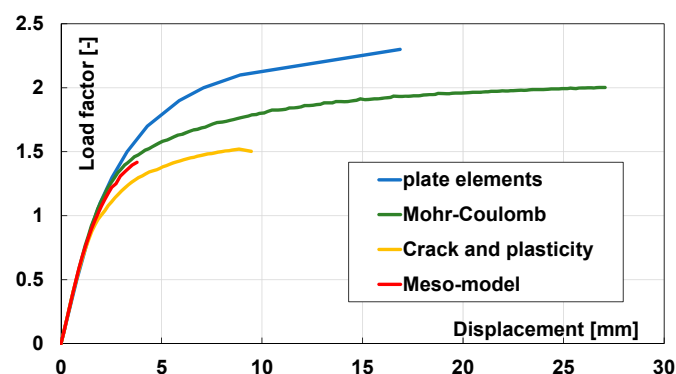


Figure 12. Horizontal displacement of pier top for various models.

From these different simulations, it can be concluded that the use of solid elements leads to a reduction of 0.84 times the failure load and the use of crack and plasticity further gives a reduction of 0.59 times the initial value. This last number does not significantly differ from the result for the meso-model with brittle behavior, for which the failure load gives 0.55 times the value of the first model. The main point is that the Mohr–Coulomb

approach fails. Going back to Equation (4), realistic values for $\tan \varphi$ are understood to be between 0.2 and 0.4, because this is the friction factor of bricks on mortar layers. Realistic values for the cohesion c vary from 0 to 0.04 MPa. The application of the Mohr–Coulomb equation for $f_c = 2$ MPa and $f_t = 0.1$ MPa gives $\tan \varphi = 2.12$ and $c = 0.224$. Neither value is realistic. Because of this, the failure by shear cannot be accurately determined using the Mohr–Coulomb equation. The brittle fracture meso-model gives $\tan \varphi = 0.3$ and $c = 0.02$. These values are certainly acceptable.

Since shear is the cause of the failure, it is evident that sophisticated models with specific features are required in this case. Should this not be the case, then even an approach with plates will already give a decent result. To clarify the mechanism, Figure 13 shows a detail of a vertical section in the pier, which clearly shows that a horizontal crack is formed due to tension. As a result, the area of the cross-section is reduced, and it collapses due to shear and not due to excessive compression.

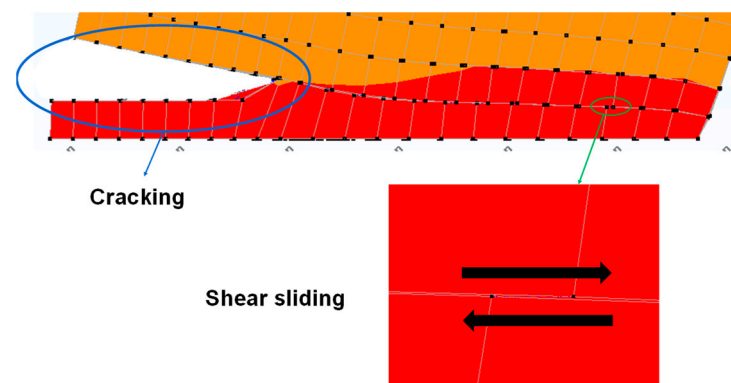


Figure 13. Vertical section of pier base with cracking and shear sliding.

It should be noted that the same conclusion is reached for the effect of debris with this elaborate model. The load at which local damage occurs increases linearly with the strength of the masonry. This local damage encourages cracking, thus fostering collapse due to torrent waves.

5. Results of Case 2: Candia Viaduct (Italy)

The Candia Viaduct crosses the Sesia River near the town of Candia Lomellina, to flow a little further into the Po. It comprises 16 spans of pressed masonry arches with an opening of 17 m. The ratio of the arrow of the arch to the gap between the arch births is only 0.153. This viaduct was investigated with monitoring because damage to the piers was found as a result of scour [21]. The width of the viaduct is 10.05 m, and the ratio of this width to the height of the top of the arches is therefore $10.05/5.58 = 1.80$. This value is considerably higher than the ratio of 0.40 for Devil’s Bridge. The front view of the viaduct is exhibited in Figure 14.

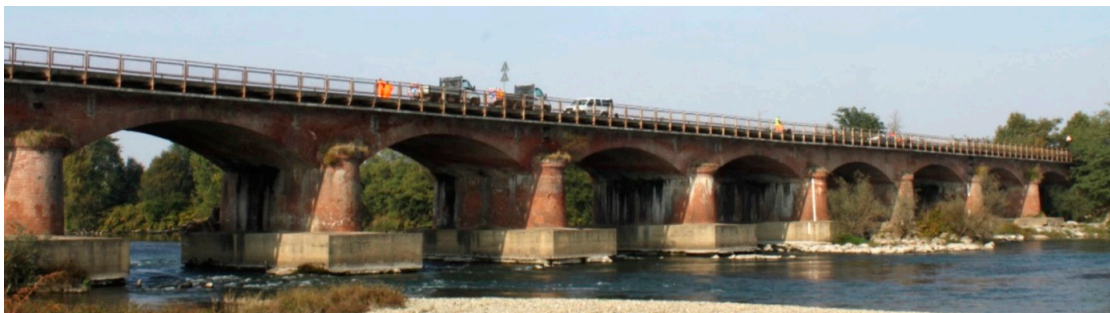


Figure 14. Candia Viaduct—front view.

As in the previous case, an approximate simulation was carried out with plate elements, the composition of which has an identical moment of resistance as the actual pier or vault.

A first observation is that the individual arches are not able to resist the dead load, and it is therefore essential that the thrust forces sufficiently compensate one other. Hence, it turned out to be necessary to model the 16 spans as a whole. The entire model is exhibited in Figure 15.

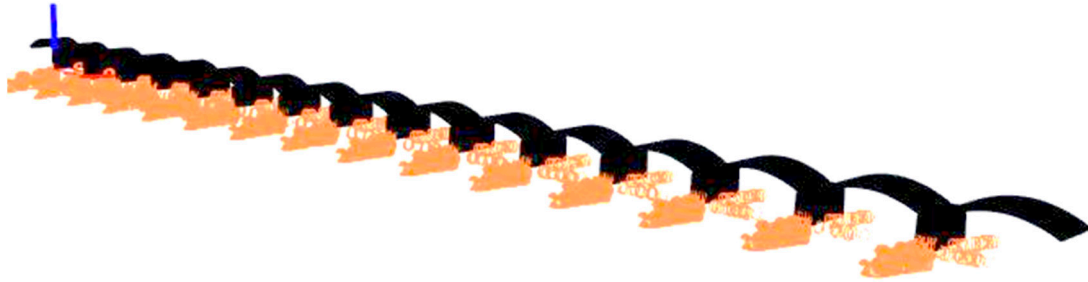


Figure 15. Model of the Candia Viaduct with plate elements, overview, and detail.

The horizontal loads also differ in intensity. The maximum water height found is only 3.50 m. In addition, there appears to be little certainty about the compressive and tensile strength of the masonry. A range of numerical values for f_c was therefore used in all cases, which varied from 3.1 to 20.3 MPa. The latter high value does not seem realistic.

The failure load was determined in the same way as in the previous case. For the case of the torrent wave, a consistent result was found, as long as the strength f_c was limited to the lowest value of 3.1 MPa. The Southwell plot for this material strength is also a quasi-linear graph that shows a failure load magnitude of 974 kN. For higher values of f_c , the graph is much too unclear, and the application of the Southwell plot fails. The vertical stresses at the base of the pier do not reach their maximum value at the ends of the cross-section but rather at a distance of 0.25 times the width of 10.50 m from the pier. This is due to the fact that the piers are wider than the vaulted arches. The vertical stress is exhibited in Figure 16, for various values of the wave height.

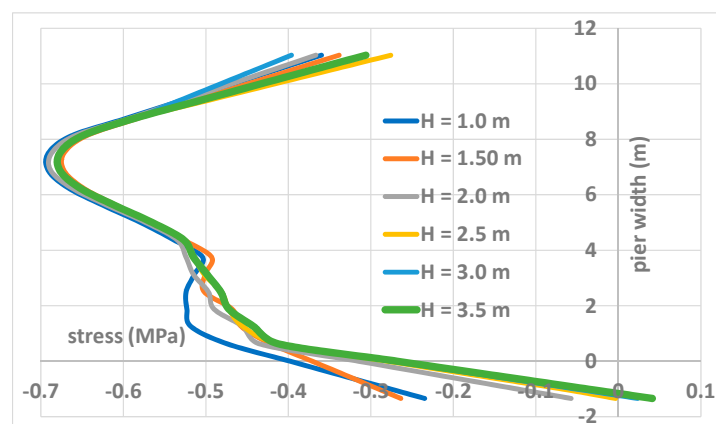


Figure 16. Vertical stress in pier cross-section with wave height.

The failure mechanism can be explained in the following way: In this case, i.e., a wide pier, the upstream pier edge may show a small amount of tension and subsequently crack. As a consequence, the compression stress continues to increase, and failure will occur through excessive compression. As the Southwell method failed for most values of masonry strength, the alternative method of tangent stiffness plot, as described in [19], was used. The results of this method, as exhibited in the graph of Figure 17, clearly indicate the increase in the failure load with compression strength. Hence, the model and the

use of the Mohr–Coulomb hypothesis are validated, and the failure load increases with compression strength.

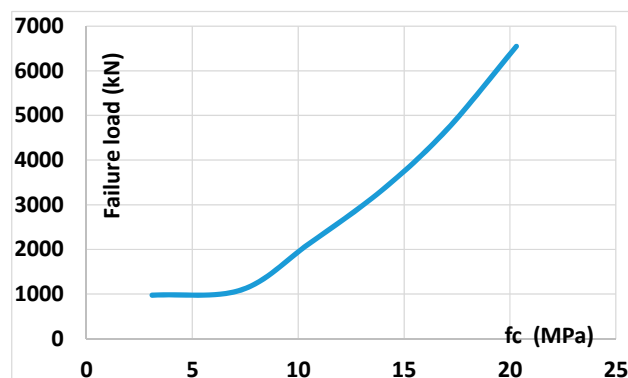


Figure 17. Failure load versus f_c .

Regarding the effect of debris load, the stress distribution, failure mechanism, and the value of the failure load are similar to the former case. Yet, the character of failure is different. As in the previous case, the local damage fosters cracking and subsequently leads to a similar failure mechanism to that of the torrent wave load.

6. Discussion

Based on two, albeit extreme, cases, it is difficult to draw general conclusions about the effects of river torrent waves and floating debris. However, this topic has become relevant, as numerous recent examples of the effects of flooding in many countries and cities demonstrate. They are all due to climate change.

What is striking about the results is that the geometry of the piers is important. The piers of Devil's Bridge are high, narrow, and slender, while those of the Candia Viaduct are short and have a large width, parallel to the river. In the latter case, it is clear that shear is not the basis of the failure mechanism. It is suspected that this corresponds to the situation of most historic masonry bridges, and the generally expected failure mechanism is that excessive compression stress is introduced at the downstream end of the pier. In addition, there is the effect of the vertical load, which avoids shear failure due to the increased vertical compression stress. This strengthens the expected failure mechanism due to excessive compression. It has been proven that shear failure is more difficult to simulate than the common cause of failure. The exact limit value of slenderness at which the transition occurs from one mechanism to the other must be further determined.

However, failure due to excessive compression certainly does not mean that the size of the failure load is proportional to the compressive strength.

Moreover, it is difficult to determine which type of load, river torrent waves or debris, is the most harmful. Both have a different effect. Torrent impact causes global failure, while debris mainly causes local damage. The latter can certainly lead to failure if the damage is not repaired in time.

In this study, no further research was carried out regarding the water pressure induced. A generic distribution of the pressure and magnitude of the forces was selected from the literature. The collapse condition was then that of an increased intensity of the same pressure or force. In reality, during a torrent flood, the water mass flows toward the constructed structure at a certain speed, and objects that collide with the pillars can have different masses. For example, slowly flowing water can carry large objects, causing heavy local damage. Global failure will not occur. A fast-flowing flood can certainly throw the structure out of balance.

If one or more spans of the bridge are narrow, and there is a significant volume of debris, general occlusion can occur, and the effect of debris might generate a larger force than the value considered in this study. This proved to be the case of the Baghetto Bridge

across the Adda River in Italy [22], where the debris accumulated against the bridge deck. There is no evidence such an occlusion has ever occurred with the Devil's Bridge. In the case of the Candia Viaduct, it seems quite probable, although no record of it was found.

Another important verification of the numerical models is updating them through vibration measurement and connected modal analysis. This requires the site measurement of frequencies and mode shapes. However, most masonry bridges have a solid character, and frequencies are expected to be high. Amplitudes are small, and the accuracy of measurement might be close to the ambient noise. Nevertheless, the present equipment allows for obtaining relevant results. In future work, this updating of the models, as in [22], will prove to be highly relevant.

7. Conclusions

It has become clear that whether torrent floods are an issue for masonry vaulted arch bridges depends on the situation. Information about the speed of the water and the mass of the debris for the local condition should greatly improve the assessment. This requires on-site recording and the possible extrapolation of the data for longer return periods. Naturally, climate change plays an important role in this.

In the future, the refinement of load values due to wave torrents and debris will be needed. This may be based on site measurements, the optimization of the numerical models, or a more precise determination of the debris force, in the case of general occlusion of a single or more spans. Finally, future work considering this aspect might result in obtaining a clear relation between the return period of wave torrents and the failure load.

In addition, the condition of the structure is important. Not only are the mechanical characteristics of the masonry important but also whether there is any local damage. The extensive testing of the compressive strength appears to be of less importance, if shear is the cause of failure, as the influence of this factor is less significant.

It is therefore certain that further research in this area considering the aforementioned factors is necessary if important bridges of cultural and historical value are to be preserved.

Author Contributions: Conceptualization, P.V.B. and H.D.B.; methodology, P.V.B.; software, H.D.B.; validation, P.V.B. and H.D.B.; formal analysis, P.V.B.; investigation, P.V.B.; resources, H.D.B.; data curation, P.V.B. and H.D.B.; writing—original draft preparation, P.V.B.; writing—review and editing, P.V.B.; visualization, P.V.B.; supervision, H.D.B.; project administration, H.D.B.; funding acquisition, None. All authors have read and agreed to the published version of the manuscript.

Funding: This research received no external funding.

Data Availability Statement: Data are contained within the article.

Acknowledgments: The authors are grateful to D. Partov from Lyuben Karavelov University Sofia (BG), N. Tuleshkov from the Bulgarian Academy of Sciences Sofia (BG), and P. Borlenghi and C. Gentile, both from Politecnico di Milano (I), for providing most of the basic material and information.

Conflicts of Interest: The authors declare no conflicts of interest.

References

1. Vokal, M.; Drahorad, M. Legion Bridge in Prague. *Trans. VSB-Tech. Univ. Ostrav. Sect. Build. Struct. Struct. Mech.* **2019**, *19*, 71–80.
2. Hellmlich, K. Determination of the load carrying capacity of masonry arch bridges based on measurements. In Proceedings of the 7th International Conference on Structural Faults and Repair, Edinburgh, UK, 8 July 1977.
3. Gilbert, M. Limit analysis applied to masonry arch bridges: State of the art and recent developments. In Proceedings of the Arch '07, the 5th International Conference on Arch Bridges, Madeira, Portugal, 12–14 September 2007; pp. 13–28.
4. Heyman, J. The stone skeleton. *Int. J. Solids Struct.* **1966**, *2*, 249–279. [[CrossRef](#)]
5. Bouzas, O.; Conde, B.; Matos, J.-C.; Solla, M.; Cabalero, M. Reliability-based structural assessment of historical masonry arch bridges: The case of Cernadela Bridge. *Case Stud. Constr. Mater.* **2023**, *18*, e02003. [[CrossRef](#)]
6. Addressi, D.; Gatta, C.; Nocera, M.; Liberatore, D. Nonlinear dynamic analysis of a masonry arch bridge accounting for damage evolution. *Geosciences* **2021**, *11*, 343. [[CrossRef](#)]
7. De Santis, S.; Felice, G. Seismic analysis of masonry arches. In Proceedings of the 15th World Conf. on Earthquake Engineering, Lisbon, Portugal, 24–28 September 2012.

8. Clemente, P.; Saitta, F.; Buffarini, G.; Ormando, C. Masonry arch bridges with finite compression strength subject to horizontal longitudinal seismic actions. *Appl. Sci.* **2023**, *13*, 7509. [[CrossRef](#)]
9. Proske, D.; Krawtschuk, A.; Zeman, O. Experimental investigation of masonry arches exposed to horizontal impact. *Mauerwerk* **2015**, *19*, 298–311. [[CrossRef](#)]
10. Zampieri, P. Horizontal capacity of single-span masonry bridges with intrados FRCM strengthening. *Compos. Struct.* **2020**, *244*, 112238. [[CrossRef](#)]
11. Van der Cruyssen, D.; Beeby, A. Lateral loading on masonry arch bridges. *Struct. Eng.* **2000**, *78*, 14–17. Available online: <https://search.worldcat.org/search?q=n2:14665123> (accessed on 10 October 2023).
12. Majtan, E.; Cunningham, L.; Rogers, B. Numerical study on the structural response of a masonry arch bridge to flood flow and debris impact. *Structures* **2022**, *48*, 782–797. [[CrossRef](#)]
13. EN 1996-1-1; Eurocode 6: Design of Masonry Structures Part 1-1—General Rules for Reinforced and Unreinforced Masonry Structures. CEN: Brussels, Belgium, 2005; (+ addendum 2009) CEN Brussels.
14. D’Altri, A.M.; De Miranda, S.; Castellazzi, G.; Sarhosis, V. A 3D detailed micro-model for the in-plane and out-of-plane numerical analysis of masonry panels. *Comput. Struct.* **2018**, *206*, 18–30. [[CrossRef](#)]
15. Van Doorslaer, K. Reduction of Wave Overtopping by and Wave-Induced Forces on Storm Walls and Promenades at Crest Level of Smooth Dikes: An Experimental Study. Ph.D. Dissertation, Ghent University, Ghent, Belgium, 2018.
16. Deutsche Gesellschaft für Geotechnik e.V. *Empfehlungen des Arbeitsausschusses Uferbefestigungen Häfen und Wasserstrassen*; Ernst u Sohn: Berlin, Germany; Hoboken, NJ, USA, 2022.
17. van Maris, B. Wave Loads on Vertical Walls: Validation of Design Methods for Non-Breaking Waves of Bimodal Spectra. Master’s Thesis, Delft University of Technology, Delft, The Netherlands, 2018.
18. Tuleshkov, N. *Bridging the Ancient and Medieval World*; Part Three. Bridges from the territory of the Ottoman Empire; Bulgarian Academy of Sciences: Sofia, Bulgaria, 2022.
19. National Institute of Meteorology and Hydrology. Study of Historical Floods in Central and Eastern Europe from an Integrated Flood Management Viewpoint. 2004. Available online: https://www.floodmanagement.info/projects/pilot/europe/Flash_Flood.Bulgaria.pdf (accessed on 22 September 2022).
20. Dos Santos, G.; Gardner, L.; Kucukler, M. A method for the numerical derivation of plastic collapse loads. *Thin-Walled Struct.* **2017**, *124*, 258–277. [[CrossRef](#)]
21. Borlenghi, P.; D’Angelo, M.; Ballio, F.; Gentile, C. Continuous Monitoring of Masonry Arch Bridges to Evaluate the Scour Action. *Lect. Notes Civ. Eng.* **2022**, *200*, 400–408. [[CrossRef](#)]
22. D’Angelo, M.; Menghini, A.; Borlenghi, P.; Bernardini, L.; Benedetti, L.; Ballio, F.; Belloli, M.; Gentile, C. Hydraulic safety evaluation and dynamic investigations of Baghetto Bridge in Italy. *Infrastructures* **2022**, *7*, 53. [[CrossRef](#)]

Disclaimer/Publisher’s Note: The statements, opinions and data contained in all publications are solely those of the individual author(s) and contributor(s) and not of MDPI and/or the editor(s). MDPI and/or the editor(s) disclaim responsibility for any injury to people or property resulting from any ideas, methods, instructions or products referred to in the content.